Inorg. Chem. **2008**, *47*, 6072−6076

New Layered Hydrogenophosphate, Protonic Conductor: $Mn(H_2PO_4)_2$

R. Baies,[†] V. Pralong,*[,†] V. Caignaert,[†] M. P. Saradhi,[†,‡] U. V. Varadaraju,[‡] and B. Raveau[†]

Laboratoire de Cristallographie et Sciences des Matériaux, ENSICAEN, Université de Caen, CNRS, 6 Bd Maréchal Juin, F-14050 Caen 4, France, and Materials Science Research Centre, Indian Institute of Technology Madras, Chennai 6000 036, India

Received March 7, 2008

A new hydrogenophosphate $Mn(H_2PO_4)_2$ has been synthesized from an aqueous solution. Its ab initio structure resolution shows that the original layered structure of this phase consists of $PO_2(OH)_2$ tetrahedra and MnO_5OH octahedra, sharing corners to form $[MnP_2O_8H_4]_\infty$ layers, whose cohesion is ensured through hydrogen bonds. The excitation and emission spectra of this phase are characteristic of Mn^{2+} species. This phosphate is shown to be a good protonic conductor with a conductivity of $10^{-4.4}$ S/cm at 90 °C (363 K).

Introduction

A great deal of theoretical and experimental work has been devoted to protonic conductors,[1−5] due to their potential as electrolyte for the production of electricity in hydrogen fuel cells.[6,7] Among these numerous materials, the layered hydrogenophosphates were revealed to be high performance materials as exemplified by the famous $HUO_2PO_4 \cdot 4H_2O$,[4,8,9] by the zirconium phosphates α-$Zr(HPO_4)_2 \cdot nH_2O$ and γ-$Zr(PO_4)(H_2PO_4) \cdot 2H_2O$,[10,11] and by the antimony phosphates $H_3Sb_3P_2O_{14} \cdot 10H_2O$ and $HSbP_2O_8 \cdot 10H_2O$.[12] Recently we investigated hydrogenophosphates of transition elements, and we showed that two of them, $VO(H_2PO_4)_2$[13] and $H_3O[Fe(H_2O)]_3[H_8(PO_4)_6] \cdot 3H_2O$,[14] characterized by a three-dimensional framework were protonic conductors. In the frame of this research, we have investigated the system Mn−P−O−H. We report herein on a new hydrogenophosphate, $Mn[PO_2(OH)_2]_2$ with an original layered structure, and we show that this phase is a protonic conductor with a conductivity close to $10^{-4.4}$ S/cm at 90 °C.

Experimental Section

The chemicals were purchased from commercial sources and used as received. The X-ray powder diffraction (XRPD) pattern was collected between 10° to 90° on a Brücker D8 diffractometer using Cu Kα radiation. The sample was loaded in a capillary ($\varnothing = 0.5$ mm) in order to limit the strong preferential orientation effect of this sample.

Thermogravimetric analysis (TGA) was performed in N_2 atmosphere at a heating rate of 2 °C/min with a TG92 Setaram microbalance. The sample morphology was studied with a scanning electron microscope (SEM) Philips Field Effect Gun (FEG) XL-30 with a resolution of about 1 nm. The cationic composition was checked by energy dispersive spectroscopy (EDS) using a kevex analyzer.

Impedance measurements were carried out with an EG&G 7220 lock-in amplifier in the frequency range 10 Hz-120 kHz. Pellets were prepared by cold pressing the powder sample. Gold electrodes were deposited by vacuum evaporation. The impedance measurements were carried out at steady state temperatures from room temperature to 90 °C under vacuum and air under 100% relative humidity (RH). Diffuse Reflectance Spectrum (DRS) of the sample was recorded using an UV−visible spectrophotometer with integrating sphere attachment (Cary Varian). $BaSO_4$ was used as the reference. Photoluminescence excitation and emission spectra at room and liquid nitrogen

* To whom correspondence should be addressed. E-mail: valerie.pralong@ensicaen.fr. Fax: +33 2 31 95 16 00. Tel: +33 2 31 45 26 32.
† Université de Caen.
‡ Indian Institute of Technology Madras.

(1) *Proton Conductors*; Colomban, Ph., Ed.; Cambridge Univ. Press: Cambridge, 1992.
(2) Clearfield, A. *Solid State Ionics* **1991**, *46*, 35–43.
(3) Kreuer, K. D. *Solid State Ionics* **2000**, *136−137*, 149–160.
(4) Barboux, P.; Morineau, R.; Livage, J. *Solid State Ionics* **1988**, *27*, 221–225.
(5) England, W. A.; Cross, M. G.; Hamnett, A.; Wiseman, P. J.; Goodenough, J. B. *Solid State Ionics* **1980**, *1*, 231–249.
(6) Alberti, G.; Casciola, M. *Solid State Ionics* **2001**, *145*, 3–16.
(7) Kreuer, K. D. *Chem. Mater.* **1996**, *8*, 610–641.
(8) Howe, A. T.; Shilton, M. G. *J. Solid State Chem.* **1979**, *28*, 345.
(9) Pham-Thi, M.; Colomban, Ph. *Solid State Ionics* **1985**, *17*, 295.
(10) Casciola, M.; Costantino, U. *Solid State Ionics* **1986**, *20*, 69.
(11) Alberti, G.; Casciola, M.; Massinelli, L.; Palombari, R. *Ionics* **1996**, *2*, 179.
(12) Deniard-Courant, S.; Piffard, Y.; Barboux, P.; Livage, J. *Solid State Ionics* **1988**, *27*, 189.
(13) Caignaert, V.; Satya Kishore, M.; Pralong, V.; Raveau, B.; Creon, N.; Fjellvåg, H. *J. Solid State Chem.* **2007**, *180* (9), 2437–2442.
(14) Pralong, V.; Caignaert, V.; Raveau, B. *Solid State Ionics* **2006**, *177* (26−32), 2453–2456.

10.1021/ic8004163 CCC: $40.75
Published on Web 06/07/2008

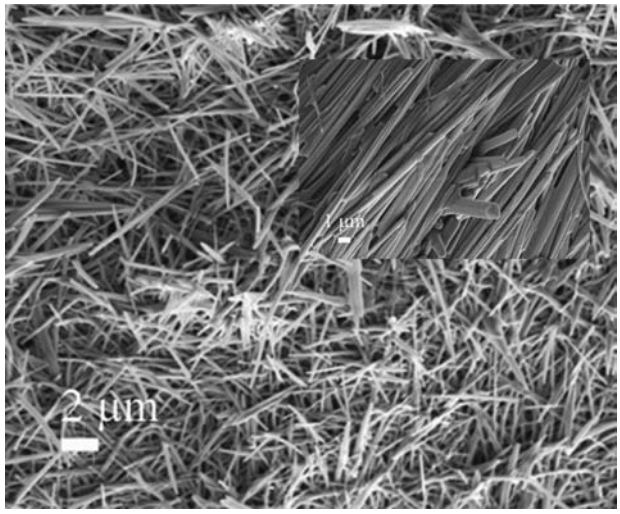

Figure 1. SEM picture of $Mn(H_2PO_4)_2$.

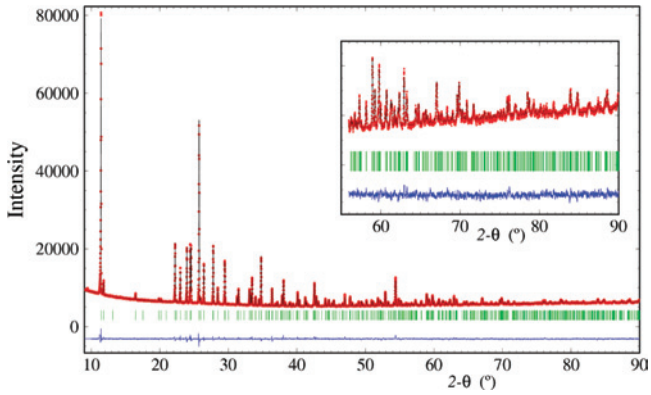

Figure 2. Rietveld refinement plot of XRD data of $Mn(H_2PO_4)_2$.

temperature were recorded on powder samples using a Horiba Jobin Yvon Fluorolog-3 spectrofluorometer having 450W xenon lamp with operating range from 220−850 nm.

Results and Discussion

Synthesis. $Mn(H_2PO_4)_2$ was synthesized from an aqueous manganese phosphate solution. Five hundred milligrams of metallic manganese (Acros, purity > 99.5%) were introduced in a borosilicate beaker containing 10 mL of H_3PO_4 (85% weight). The solution was stirred at room temperature until the metal was dissolved, and then was heated up to 200 °C while stirring. A white precipitate appeared after about 1 h. The precipitate was washed with pure acetone and filtered. The product was kept in a desiccator in order to avoid hydration. The analysis of the morphology by SEM showed that this monophosphate forms needles of about 0.1μm × 0.1μm × 10 μm length (Figure 1) The EDS analysis led to the ratio Mn/P = 1:2.

Structure Determination. The powder X-ray diffraction (XRD) pattern of this new phosphate (Figure 2) is identical to the patterns published in the PDF file (n°036−0209 and 040−0070), which remained unindexed up to the present investigation. In a first step, the first 15 peaks of the XRD pattern were indexed using the DICVOL44 program, leading to a monoclinic cell with a figure of merit M(15) = 67.3.

Table 1. Crystallographic Data for $Mn(H_2PO_4)_2$

formula sum	$Mn(H_2PO_4)_2$
formula weight	248.94 g/mol
crystal system	monoclinic
space-group	$P12_1/c1$ (14)
cell parameters	a = 7.5573(1) Å, b = 15.4540(2) Å, c = 5.4021(1) Å, β = 97.854(6)°
cell volume	625.01(1) Å^3
Z	4
calc. density	2.606 g/cm^3

Table 2. Fractional Atomic Coordinates and Isotropic Thermal Factors for $Mn(H_2PO_4)_2$

atom	Wyck.	x	y	z	B [Å^2]
Mn1	4e	0.2098(2)	0.5043(9)	0.1818(4)	0.004(39)
P1	4e	0.6049(4)	0.8885(2)	0.8033(5)	0.168(46)
O1	4e	0.4341(9)	0.9151(3)	0.6408(11)	0.907(54)
O2	4e	0.6522(8)	0.9240(3)	1.0612(8)	0.907(54)
O3	4e	0.7604(6)	0.9059(3)	0.6133(9)	0.907(54)
O4	4e	0.5992(7)	0.7855(3)	0.8290(10)	0.907(54)
H1	4e	0.597	0.772	0.635	
P2	4e	0.1009(4)	0.8739(1)	0.1512(6)	0.168(46)
O5	4e	0.0545(8)	0.9291(2)	0.3604(8)	0.907(54)
O6	4e	0.0753(7)	0.9061(3)	−0.1178(10)	0.907(54)
O7	4e	0.3113(7)	0.8487(3)	0.2304(9)	0.907(54)
O8	4e	−0.0039(6)	0.7838(3)	0.1675(10)	0.907(54)
H2	4e	0.010	0.749	0.014	

Then the space group was found to be $P2_1/c$ with the help of the CHECKCELL program.

The ab initio structure determination was performed in the real space, parallel tempering algorithm with the FOX program using PO_4 tetrahedra as chemical information in order to reduce the number of possible solutions. In these conditions, the algorithm converged to a reasonable structure and then, the model was further refined by the Rietveld method with the FULLPROF program. The refinement was conducted with 48 parameters including 36 atomic and thermal parameters. At the end of the refinement, two hydrogen sites were located geometrically, and the positions of these two hydrogen sites have been included in the structural model. The refinement converged with a weighted average Bragg R-factor of 0.072 for the atomic parameters listed in Table 1.

Description of the Structure. The bond valence sum calculations according to Alternatt and Brown[15] are given in Table 2. They show that practically one charge is missing on O3, O4, O7, and O8, so that these atoms are in fact protonated, forming OH groups. As a consequence, the two P1 and P2 atoms form tetrahedra that can be formulated as $PO_2(OH)_2$. One of these four oxygen sites (O3) is also bonded to Mn, and thus, the Mn coordination can be described as MnO_5OH octahedra.

The perspective view of the structure along c (Figure 3a) shows that it is built up of $PO_2(OH)_2$ tetrahedra sharing corners with MnO_5OH octahedra. These polyhedra form $[MnP_2O_8H_4]_\infty$ layers stacked along b, whose cohesion is ensured through hydrogen bonds. The projection of one $[MnP_2O_8H_4]_\infty$ layer along b (Figure 3b) shows that two Mn octahedra share edges forming "$Mn_2O_8(OH)_2$" bioctahedral units interconnected through $PO_2(OH)_2$ tetrahedra. Thus, each P1 tetrahedron shares three apexes with three different

(15) Brown, I. D.; Alternatt, D. *Acta Crystallogr.* **1985**, *B41*, 244.

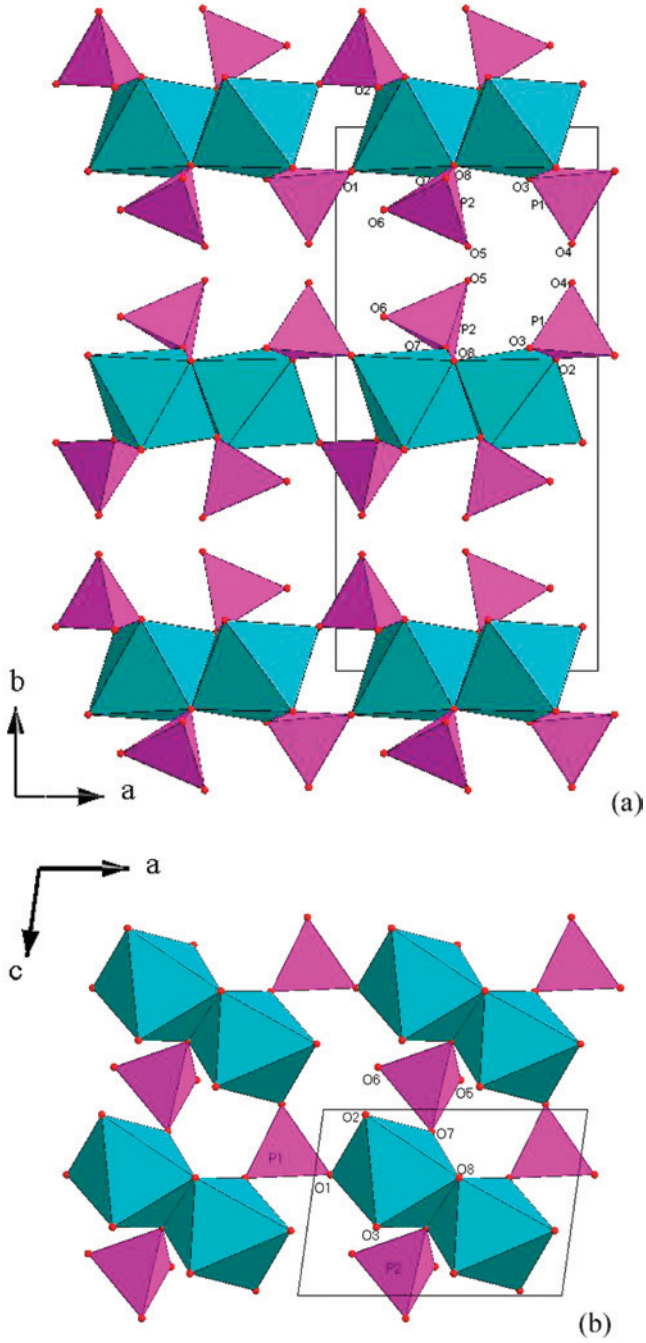

Figure 3. Crystal structure view of $Mn(H_2PO_4)_2$ along the *c* axis.

bioctahedral "Mn2" units (O1, O2, and O3), so that one OH group (O3) is shared between one P1 tetrahedron and one Mn octahedron. The second OH group of the P1 tetrahedron sits on its free apex (O4). The second tetrahedron P2 has two free apexes, O7 and O8, both occupied by OH groups, whereas the two other apexes (O5, O6) are shared with two "Mn2" bioctahedral units. Each layer can be described as built up of double ribbons $[Mn_2P_8O_{16}H_8]_\infty$ running along *c* and connected to each other laterally through the corners of their polyhedra.

The interatomic distances (Table 3) show that manganese is in a nearly regular octahedral coordination with Mn−O distance ranging between 2.05 and 2.30 Å. The two $PO_2(OH)_2$ tetrahedra have the same distortion with two short

Table 3. Selected Distances and Calculated Valences for $Mn(H_2PO_4)_2$

bond	length	atom	valence sum calc (exp)
Mn1−O1	2.155(16)	Mn1	2.14 *(2.0)*
O2	2.051(12)	P1	4.66 *(5.0)*
O3	2.246(14)	O1	1.67 *(2.0)*
O5	2.299(14)	O2	1.90 *(2.0)*
O5	2.216(12)	O3	1.16 *(2.0)*
O6	2.116(15)	O4	1.08 *(2.0)*
P1−O1	1.520(17)	P2	4.77 *(5.0)*
O2	1.491(13)	O5	1.95 *(2.0)*
O3	1.671(16)	O6	1.73 *(2.0)*
O4	1.687(13)	O7	1.02 *(2.0)*
P2−O5	1.499(14)	O8	1.05 *(2.0)*
O6	1.515(16)		
O7	1.609(15)		
O8	1.598(13)		

P−O bonds (1.49 to 1.52 Å) and two longer P−OH bonds (1.59 to 1.67 Å). The four hydrogen atoms cannot be located from XRD; nevertheless, two of them can be deduced by the analysis of the hydrogen-bond network. We found thus that the hydrogen atoms are located between the $[MnP_2O_8H_4]_\infty$ layers forming zigzag chains of O−H···O bonds along *c* (Figure 7b).

Thermogravimetric Analysis. The thermogravimetric analysis for the $Mn(H_2PO_4)_2$ sample carried out in nitrogen flow (Figure 4), shows a large weight loss occurring at 200 °C in two steps. As confirmed by XRD, this weight loss is attributed to the departure of 2 moles of water, leading to the formation of $Mn_2P_4O_{12}$.

$$Mn(H_2PO_4)_2 \rightarrow H_2MnP_2O_7 + H_2O \rightarrow Mn(PO_3)_2 + 2H_2O \quad (1)$$

Optical Properties of $Mn(H_2PO_4)_2$. Figure 5 shows Diffuse Reflectance Spectra (inset) and photoluminescence (PL) excitation spectra of $Mn(H_2PO_4)_2$. The PL excitation spectra monitored at 605 nm emission wavelength was found to be very similar to those generally observed for Mn^{2+} in octahedral coordination.[16,17] Several absorption bands, which are associated with transitions of Mn^{2+} from the $^6A_{1g}$ (S) ground-state to the excited states, are shown in the excitation spectra. A band at 240 nm in the DRS is attributed to host lattice absorption. The PL emission spectra at RT and liquid nitrogen (inset) temperature under 400 nm excitation wavelength (Figure 6) consist of two broad emission bands at 450 nm (blue) and 605 nm (red) regions. The observed

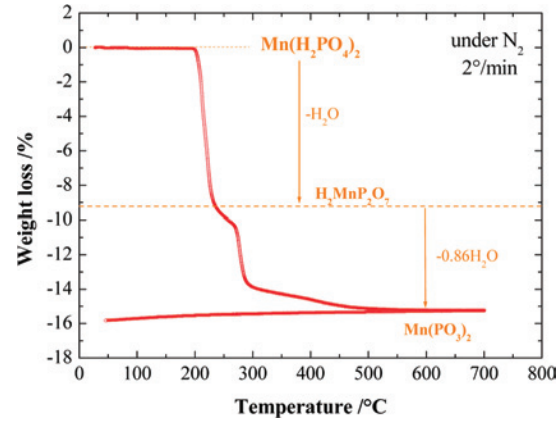

Figure 4. TGA curve of $Mn(H_2PO_4)_2$ under nitrogen flow.

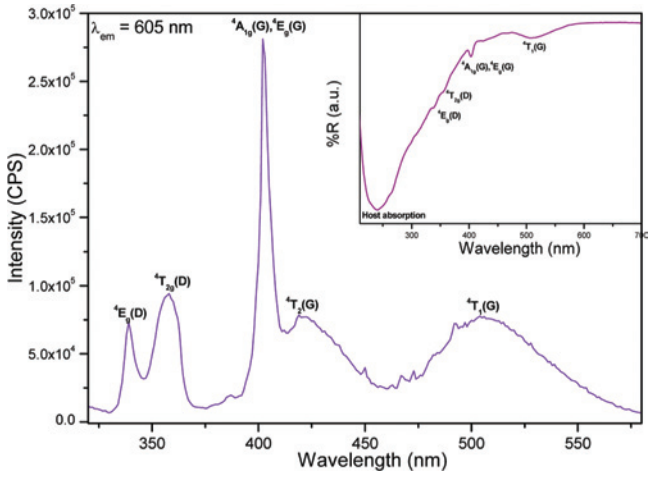

Figure 5. Excitation spectrum of $Mn(H_2PO_4)_2$, inset shows the DRS spectrum of the same.

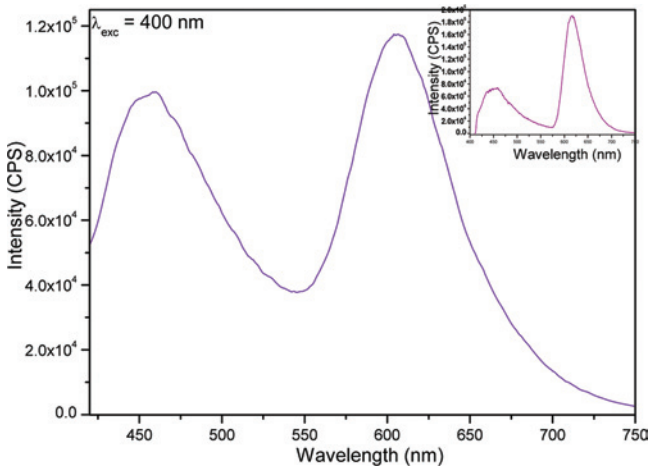

Figure 6. Emission spectra of $Mn(H_2PO_4)_2$, inset shows the emission spectrum at liquid nitrogen temperature.

emission bands are in good agreement with the Mn^{2+} emission in phosphates.[18]

Ionic Conduction Properties of $Mn(H_2PO_4)_2$. The impedance plots (Nyquist) were obtained for $Mn(H_2PO_4)_2$ between 10 Hz to 120 kHz under vacuum and air with RH = 100%. The compound was studied between room temperature and 95 °C because of its poor thermal stability. In addition, the sample reacts with water at about 95 °C to form a viscous paste which was identified as $Mn(H_2PO_4)_2 \cdot 2H_2O$ by XRD. Nevertheless, before this reaction, it is clear that the relative humidity contained in the air improves the conductivity. Moreover, a semi circle is observed at high frequency, followed by a spike at the low frequency region (inset Figure 7). The conductivity increases with temperature, reaching $10^{-4.4}$ S/cm at 90 °C (363K) under RH = 100%. The plot of Log(σ) under vacuum versus $1/T$ (Figure 7a) exhibits a linear behavior, characteristic of the classical Arrhenius relation. It evidently has only one regime of conductivity characterized by an activation energy E_a=0.47 eV. These results clearly establish that this layered manganese hydrogenophosphate is a good protonic conductor. It is of course not possible to detect what hydrogen atoms are

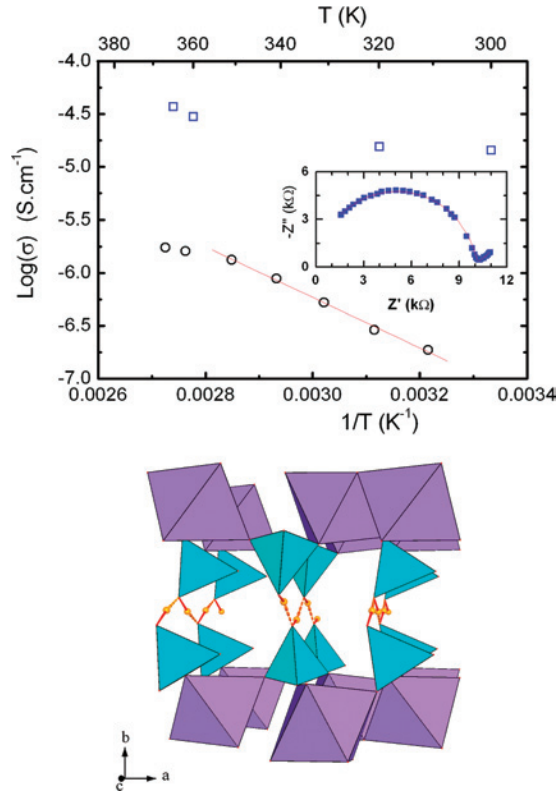

Figure 7. (a) Arrhenius plot Log(σ) versus $1/T$ of $Mn(H_2PO_4)_2$ under vacuum (○) or air RH = 100% (□). Inset: Nyquist plots of $Mn(H_2PO_4)_2$ at 87 °C. (b) Structural view of the $[MnP_2O_8H_4]_\infty$ layers: the possible diffusion path associated with successive jumps of proton ions is symbolized by dashed lines.

those responsible for the conduction and then to determine the exact nature of the conductivity, that is, to distinguish surface conductivity from bulk conductivity. But the same range of ionic conductivity was found for the compounds mentioned above.[4,8–14] For example, the layered $H_3Sb_3P_2O_{14} \cdot 10H_2O$ exhibits an ionic conductivity of 10^{-4} S/cm at room temperature with an activation energy E_a = 0.43 eV.[12] It is also worth noting that, especially in layered type structures,[12] a clear understanding of the protonic conductivity origin is rather difficult and strongly depends on the experimental condition. Nevertheless, it must be emphasized that the hydrogen atoms which are located at the border of the layers, that is, which are linked to the oxygen atoms O4 and O8 (Figure 3) are susceptible to form rather short hydrogen bonds (~1.9Å), in such a way that one OH group of one layer forms short hydrogen bonds with the adjacent layer. Thus, it is most probable that these protons may move rather easily between the $[MnP_2O_8H_4]_\infty$ layers (Figure 7b).

Conclusions

This study shows that the hydrogenophosphates represent a family of compounds with great potential for the

(16) Marco de Lucas, M. C.; Rodriguez, F.; Prieto, C.; Verdaguer, M.; Güdel, H. U. *J. Phys. Chem. Solids* **1995**, *56*, 995.
(17) Ramirez-Serrano, J.; Madrigal, E.; Ramos, F.; Caldiño, U. *J. Lumin.* **1997**, *1*, 169.
(18) Kaplanova, M.; Trojan, M.; Brandova, D.; Navratil, J. *J. Lumin.* **1984**, *29*, 199.

generation of new proton conductors, with performances similar to those previously observed for antimony phosphates. There is no doubt that the association of transition metal elements to hydrogenophosphates groups offers an immense scope to generate new proton conducting frameworks. The role of the layered character of the structure and of the presence of "O−H···O−H···" infinite chains in the protonic conduction of these phases remains an open question.

Acknowledgment. The authors want to thank S. Rey for technical help. They gratefully acknowledge the CNRS and European Union through the Novelox program, the network of excellence FAME and IFCPAR (Indo-French Centre for the Promotion of Advanced Research/Centre Franco-Indien Pour la Promotion de la Recherche Avancee), and LAFICS program for financial support through their Research, Strategic, and Scholarship programs.

IC8004163